Interferometric approach to solve microring resonance splitting in biosensor applications

S. Werquin[1] and P. Bienstman[1]

[1] Photonics Research Group, Dept. of Information Technology, Gent University, Sint-Pietersnieuwstraat 41, 9000-B Gent Belgium

Silicon-on-insulator microring resonators have proven to be an excellent platform for label-free nanophotonic biosensors. The high index contrast of the silicon-on-insulator platform allows for fabrication of micrometer size sensors. However, it also limits the quality of the resonances by introducing an intrinsic mode-splitting. Small deviations from perfect symmetry lift the degeneracy of the normal resonator modes. This severely deteriorates the quality of the output signal. The quality of the resonances is of utmost importance to determine the performance of the microrings as a biosensor. We suggest an integrated interferometric approach to give access to the unsplit, high-quality normal modes of the microring resonator.

Introduction

Silicon-on-insulator (SOI) microring resonators have proven to be an excellent platform for label-free nanophotonic biosensors. The high index contrast of the SOI-platform allows for fabrication of micrometer size sensors. The small sensor size makes microring resonators excelent candidates for highly multiplexed assays [1]. It also allows for integration of a sensor on an optical fiber tip, opening the door to in-vivo applications [2]. By combining microrings in advanced sensing configurations, it is also shown that their sensitivity can be improved significantly [3]. The high index contrast of the SOI-platform causes high confinement of the optical fields in the waveguides, which makes the microrings very sensitive to changes on the waveguide surface. This explains their very high sensitivity, but at the same time, waveguide roughness causes scattering of the guided light. This degrades the quality factor of the resonances and can ultimately lead to splitting of a resonance [4]. Because the detection limit of a microring biosensor is directly related to the quality of the ring resonance, a high Q-factor is of primordial importance in sensing applications [5]. In this paper, we present an integrated interferometric approach to resolve the resonance splitting of a microring resonantor on a single chip. Resulting in a significant improvement of the resonance quality.

Origin of resonance splitting

A perfectly symmetric microring resonator mode is twofold degenerate. Both clockwise (CW) and counterclockwise (CCW) propagation are possible in the microring and both modes are uncoupled. This degeneracy is lifted when the CW-mode and CCW-mode become coupled. Surface roughness on the waveguide edges and the proximity of bus waveguides for microring interrogation form deviations from circular symmetry. These

deviations cause forward propagating light to scatter back into the opposite direction, exciting a CCW-mode from a CW-mode and vice versa. Standing-wave modes as a symmetric and antisymmetric superposition of the traveling waves can be considered as the new eigenmodes of the system. They will however, no longer be degenerate as a consequence of the symmetry breaking coupling [6]. If the linewidth of the resonance is small enough to distinguish both modes, the resonance splitting will be visible in the output signal. This occurs for high quality resonances. Evidence of this effect is provided in figure 1, which shows both the pass-port and add-port spectrum of a microring in add-drop configuration. Only the input port is excited, so ideally, no power is present in the CCW-mode and the add-port remains dark. The measurement shows that backscattering in the microring waveguide cannot be neglected, resulting in significant power in the add-port and resonance-splitting in the pass-signal.

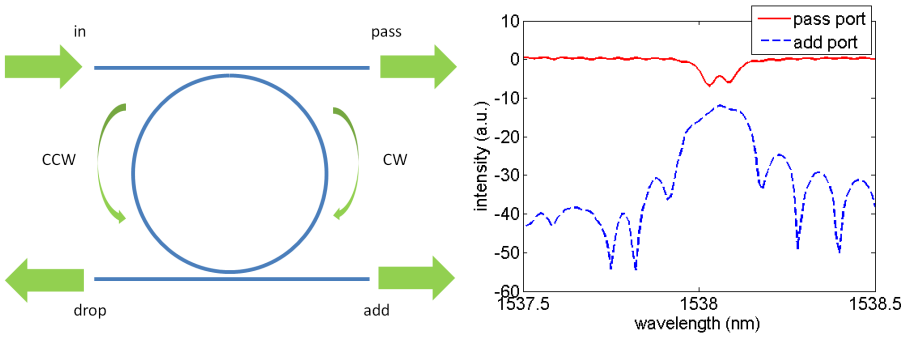

(a) (b)

Figure 1: (a) Microring resonator in add-drop configuration (b) Measured spectra showing resonance splitting and backscattered power

Integrated interferometric circuit

As demonstrated in [7], an interferometric approach can be used to access the normal modes of the microring resonator in an output signal. We have implemented this in an integrated circuit on a single SOI-chip. A layout of the circuit is provided in figure 2. Vertical grating couplers are used to couple light from a tunable laser lightsource into

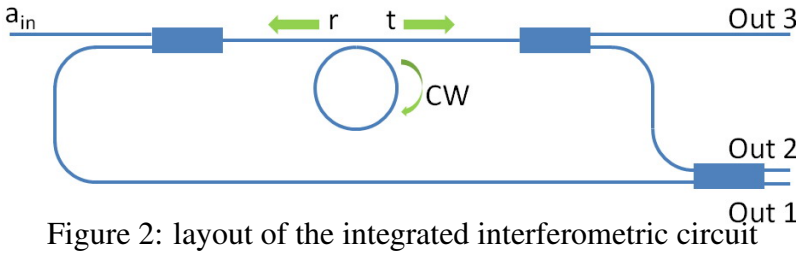

Figure 2: layout of the integrated interferometric circuit

the circuit and collect the power at the output. The input light excites a CW-mode in the microring resonator, a CCW-mode is excited as a consequence of mode-coupling. The normal modes of the microring are a symmetric and antisymmetric superposition of the CW and CCW-mode, so we can express them as follows:

$$a_{\pm} = \frac{1}{\sqrt{2}}(a_{CW} \pm a_{CCW}) \quad (1)$$

If the coupling per unit time between the bus waveguide and the microring is represented by κ, the fields transmitted and reflected by the resonator are

$$t = \frac{1}{\sqrt{2}} a_{in} + \kappa a_{CW} \quad \text{and} \quad r = \kappa a_{CCW} \tag{2}$$

Both fields are combined in a multi mode interferometer (MMI), this results in the following signals at the different output ports. ϕ denotes the phase difference between the combining waves.

$$\begin{aligned} out_1 &= \tfrac{1}{2}(\tfrac{1}{\sqrt{2}} a_{in} + \kappa a_{CW} + e^{i\phi} \kappa a_{CCW}) \\ out_2 &= \tfrac{1}{2}(\tfrac{1}{\sqrt{2}} a_{in} + \kappa a_{CW} - e^{i\phi} \kappa a_{CCW}) \\ out_3 &= \tfrac{1}{\sqrt{2}} t \end{aligned} \tag{3}$$

If we design the circuit such that the phase difference between the reflected and transmitted wave equals a multiple of 0 or π, we see that the signals in output one and two are proportional to the normal modes of the resonator. At the same time, output three is proportional to the pass-signal of the microring resonator in the all-pass configuration. This means we have access to the unsplit, high-Q normal modes of the cavity. If the detection limit of a biosensor is limited by the quality-factor of the resonance, this provides a tool to improve the detection limit significantly. Higher resonator Q-factors give rise to lower detection limits.

Experimental results

The circuit from figure 2 is designed and processed in a CMOS pilot line at imec. Using the vertical in- and outputcouplers on the waveguides, the chip can easily be measured in a fiber-to-fiber configuration. For the junction regions where waveguides are combined and splitted, MMI 2x1 and MMI 2x2 couplers are used. The coupling from the microring to the waveguide is ensured by weak evanescent coupling to a neighbouring bus waveguide. To obtain the measured spectra, a SANTEC TSL-510 Tunable laser source is used to generate the input signals. Output intensities are measured by a HP-8153 optical powermeter. The laser wavelength is swept in $10pm$ steps during recording of the power.
Figure 3 shows the recorded specta at the three outputs of the circuit. Output one and two are proportional to the normal modes of the resonator, output three returns the all-pass spectrum. We clearly see the all-pass spectrum shows severe splitting of $60pm$ in the resonance. This values is comparable to 3dB-bandwidth of the normal mode in output one. The Q-factors of the recorded resonances are listed in table 1. This result shows

Table 1: Q-factors of resonances

resonance	Q-value
output 1	$2.20 \cdot 10^4$
output 2	$1.05 \cdot 10^4$
output 3	$1.28 \cdot 10^4$

an almost twofold improvement of the resonance quality from output three to output one. Notice the distinct asymmetrical shape of the resonance in output two which makes unambiguous definition of a Q-value difficult. Additionally, the extracted normal modes do not correspond exactly with the normal modes we can distinguish in the all-pass signal. This non-ideal behaviour is a consequence of fabrication variations. The 2x2 MMI is

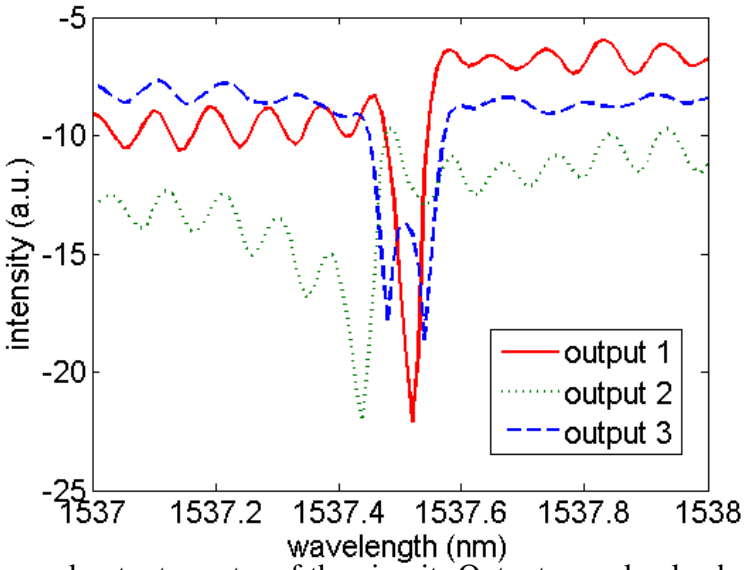

Figure 3: Measured output spectra of the circuit. Output one clearly shows the improvement of the resonance shape compared to the all-pass signal in output three.

especially sensitive to this and is not exactly balanced as a result. Also the phase relation between the reflected and the transmitted wave differs slightly from the required value of $k \cdot \pi$. This can be solved by careful tuning of the waveguide structures.

Conclusion

We have succesfully integrated an interferometric setup to resolve the resonance splitting of microrings on the SOI-platform. The access to the unsplit normal modes of the resonator allows the improvement of the detection limit of microring resonator biosensors.

References

[1] K. De Vos, J. Girones, T. Claes, Y. De Koninck, S. Popelka, E. Schacht, R. Baets, and P. Bienstman, "Multiplexed Antibody Detection With an Array of Silicon-on-Insulator Microring Resonators," *IEEE Photonics Journal*, vol. 1, no. 4, pp. 225–235, Oct. 2009.

[2] C. L. Arce, K. D. Vos, T. Claes, K. Komorowska, D. V. Thourhout, and P. Bienstman, "Silicon-on-insulator microring resonator sensor integrated on an optical fiber facet," *IEEE Photonics Technology Letters*, vol. 23, no. 13, pp. 890–892, 2011.

[3] T. Claes, W. Bogaerts, and P. Bienstman, "Experimental characterization of a silicon photonic biosensor consisting of two cascaded ring resonators based on the Vernier-effect and introduction of a curve fitting method for an improved detection limit," *Optics Express*, vol. 18, no. 22, pp. 22 747–22 761, 2010.

[4] W. Bogaerts, P. D. Heyn, T. V. Vaerenbergh, K. D. Vos, S. Kumar, T. Claes, P. Dumon, P. Bienstman, D. V. Thourhout, and R. Baets, "Silicon Microring Resonators," *Laser & Photonics Reviews*, vol. 6, no. 1, pp. 47–73, 2011.

[5] T. Claes, J. Molera, K. De Vos, E. Schacht, R. Baets, and P. Bienstman, "Label-Free Biosensing With a Slot-Waveguide-Based Ring Resonator in Silicon on Insulator," *IEEE Photonics Journal*, vol. 1, no. 3, pp. 197–204, Sep. 2009.

[6] T. J. Kippenberg, S. M. Spillane, and K. J. Vahala, "Modal coupling in traveling-wave resonators." *Optics letters*, vol. 27, no. 19, pp. 1669–71, Oct. 2002.

[7] J. Knittel, T. G. McRae, K. H. Lee, and W. P. Bowen, "Interferometric detection of mode splitting for whispering gallery mode biosensors," *Applied Physics Letters*, vol. 97, no. 12, p. 123704, 2010.

Modeling of the Raman Effect in a Silicon Photonic Crystal Cavity

Antonia Paolicelli, Benedetto Troia, Francesco De Leonardis,
and Vittorio M. N. Passaro

Photonics Research Group, Dipartimento di Elettrotecnica ed Elettronica, Politecnico di Bari, Italy.

In this paper a detailed modeling of enhancement of the Raman effect in a silicon photonic crystal slab cavity with a hexagonal lattice of air holes is presented. After investigating the cavity modes for various cavity geometries, we derive the generation of Stokes waves in the silicon inside the cavity mode, using a time domain model and assuming a Fabry-Perot type cavity. The analysis is performed as a function of cavity length, wavelength, hole radius, and cladding medium (air or water). An enhancement of 30 times in air and an output Stokes efficiency of 5% are so theoretically proven.

1. Introduction

Nonlinear optics is a broad field of research and technology that has proven to be versatile for different applications such as telecommunications and optical sensing, but until now only a few studies have associated nonlinear effects with photonic crystal structures. In this work, the generation of the Raman effect in a device based on photonic crystal structure is theoretically investigated.

2. PhC Structure

Starting from the cavity in a photonic crystal used for trapping of bacteria in water [1], the work has been developed to generate the Raman effect. The structure is shown in Fig. 1, where a number of numerical parameters used in mathematical model are evidenced. An hexagonal pattern of air holes is embedded on a silicon-on-insulator (SOI) platform with silicon slab thickness of 220 nm; the lattice constant is $a = 430\ nm$, the radius of holes is $r = 0.3a$. To make the cavity region, six holes have been removed at the center of the structure, as well as the inner holes have been shifted outward by an amount of $s = 0.2a$ to obtain a cavity length $L = 2.9\ \mu m$.

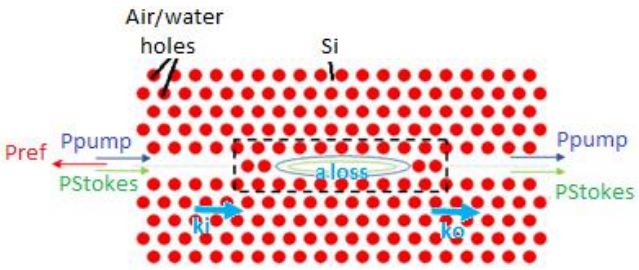

Fig.1. Cavity structure with main parameters of model: pump power (blue), Stokes power (green) and reflected power (red); input (ki) and output (ko) coupling coefficients, and cavity losses (aloss), used in the mathematical model.

3. Model and Results

The structure performance have been evaluated using two different cladding media, air and water. This choice is due to the possibility of using the device for sensing in aqueous environment, in addition to the gaseous one. The device has been studied by a

2D FDTD software (RSoft CAD), using the effective index method to mimic a 3D PhC structure. The resonance behavior has been found by launching a Gaussian pulse of a power of 1 W. Only for TE mode excitation the structure has shown significant results. Obviously, the resonant peak shows a red shift with changing the cover medium from air ($n = 1$) to water ($n = 1.318 @ \lambda = 1550\ nm$).
On the basis of a spectral analysis, both reflectance, transmittance and resonance have been investigated at the input, output and in cavity region, respectively. Changing homogeneously the radius of holes, it has been possible to collect complete information about the spectral behavior of device. All results have been later imported and processed by numerical software to implement the mathematical model. The mathematical model used to simulate the Raman effect [2] is based on two differential equations in the time domain for the nonlinear coupling between pump and Stokes wave, including two photon absorption (TPA) and free carrier absorption (FCA) effects. The model was originally applied only to a ring resonant cavity, but in this work it has been adapted to the photonic crystal sketched in Fig. 1, which is comparable to a Fabry - Perot cavity. Firstly, we have investigated the performance of a Raman laser in CW regime keeping to zero the Stokes probe at the waveguide input. Secondly, the potential of pulsed Raman amplification has been analysed when a Stokes probe is present.
An appropriate set of coefficients has been evaluated by which it is possible to describe the portion of power transferred from the input guide to the cavity (k_i) and from the cavity to the output (k_o), as well as the amount of losses of the cavity (a_{loss} in Fig. 1). These coefficients have been calculated by FDTD simulations. In particular, they have been derived from the spectral function evaluated at the output and inside the PhC cavity. The geometrical cavity characteristics have been derived by comparing the cavity to a Fabry-Perot structure, to match the resonance peaks in the same range of wavelengths, when pump and Stokes waves are launched into the cavity, with length:

$$L = \frac{\pi c m}{n_p \omega_p - n_s \omega_p + n_s \Omega_R} = 2.9\ \mu m \tag{1}$$

where ω_p is the pump resonant frequency, n_p and n_s are the refractive indices of medium seen by pump and Stokes wave, respectively, $\Omega_R = 15.6\ THz$ is the Raman shift for silicon and m is the resonance order. This condition is needed to minimize the off-resonance effects and improve the device performance.
Resonant wavelenghts have been calculated for Stokes and pump signals, initially. The PhC cavity described above exhibits the operative wavelength $\lambda = 1.484\ \mu m$ (pump wave) and a third order resonance. On the contrary, when the Stokes wave at $\lambda \cong 1.634\ \mu m$ is generated into the cavity, the sensor exhibits only two resonant peaks, one of them being in the same spectral range as previously obtained in case of input pump wave, around $\lambda \cong 1.63\ \mu m$. The parametric analysis has been executed by considering homogeneous variation of holes radii, in order to explore the sensor operation as a function of different geometrical arrangements, thus to identify the optimal cavity design. Simulation results for output transmittance are plotted in case of air and water cladding for pump and Stokes waves in Fig. 2 and Fig. 3, respectively.

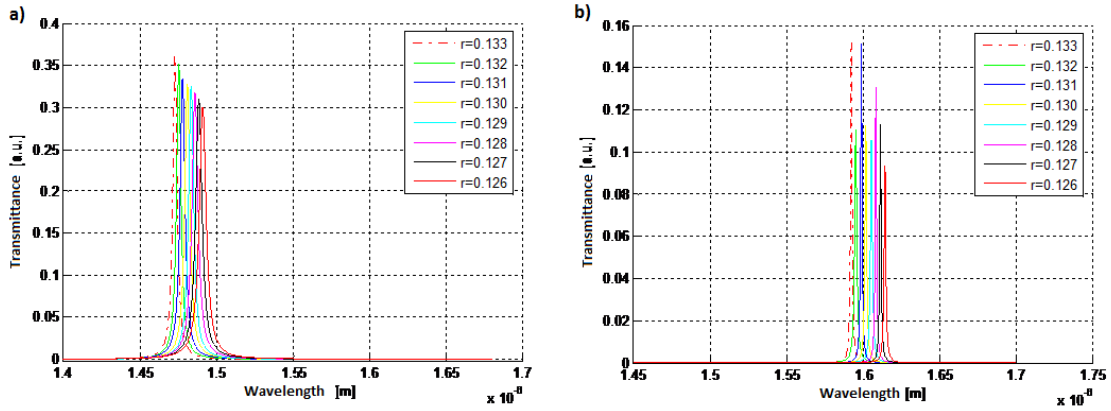

Fig. 2. Transmittance output in case of air cover for pump (left) and Stokes wave (right).

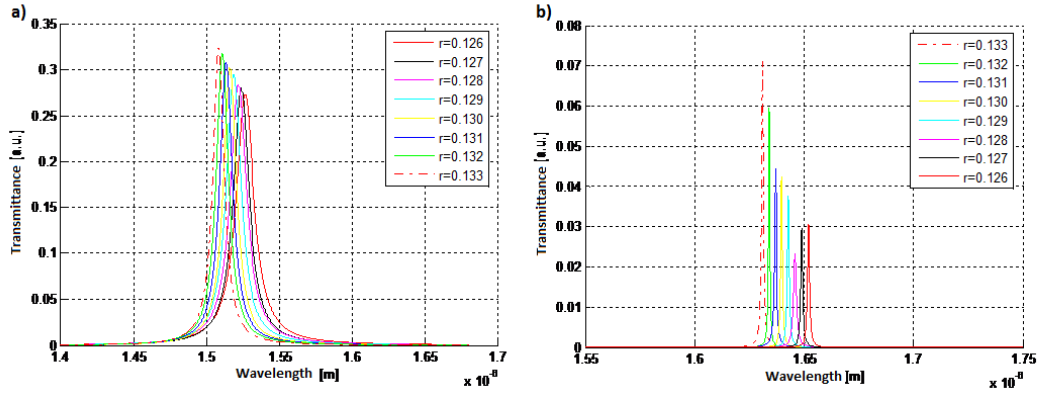

Fig. 3. Transmittance output in case of water cover for pump (left) and Stokes wave (right).

In Tables 1 and 2, coupling coefficients are listed only for pump and Stokes wave for air cladding, but similarly the coefficients for water cover have been obtained, giving an high input coupling and low output coupling, as well as a good optical field confinement in the PhC cavity. In addition, propagation losses inside the cavity are quite high, influencing the signal output power. In fact, propagation losses have been estimated in different simulations, allowing to eliminate the propagation loss contribute from the parameter a_{loss}.

Radius[μm]	***Wavelength [μm]***	***k_i (%)***	***k_o (%)***	***aloss[dB/cm]***
r = 0.126	1.491	11.2	0.84	18
r = 0.127	1.489	10.5	0.82	18
r = 0.128	1.486	9.7	0.78	18
r = 0.129	1.483	8.5	0.71	18
r = 0.130	1.481	8.35	0.71	18
r = 0.131	1.478	7.95	0.69	18
r = 0.132	1.475	7.3	0.67	18
r = 0.133	1.473	7	0.66	18

Table 1. Coupling coefficients and loss factors evaluated by FDTD simulations for pump wave in case of air cladding.

By simulating the PhC sensor with two different cladding media (i.e., air or water), it is possible to affirm that the common effect consists in the shift of resonant wavelength peaks for pump and Stokes waves, but that shift is different.

Radius[μm]	*Wavelength[μm]*	k_i *(%)*	k_o *(%)*	*aloss[dB/cm]*
r = 0.126	1.614	3.58	0.08	18
r = 0.127	1.611	2.09	0.06	18
r = 0.128	1.608	2.46	0.079	18
r = 0.129	1.606	3.05	0.077	18
r = 0.130	1.602	2.91	0.08	18
r = 0.131	1.599	1.98	0.078	18
r = 0.132	1.595	3.8	0.1	18
r = 0.133	1.592	2.1	0.082	18

Table 2. Coupling coefficients and loss factors evaluated by FDTD simulations for Stokes wave in case of air cladding.

Finally, another device with a cavity length of several hundreds of microns, corresponding to a very large resonant order from Eq. (1), has been studied and the amount of Stokes power collected at the device output has been accurately estimated. The results obtained by this type of cavity have shown that an amount of Stokes power could be guided from the PhC structure output with an efficiency around 5%.

4. Conclusions

In conclusion, the investigated device evidences intriguing potentialities for sensing performance as a new class of PhC sensors based on nonlinear effect (i.e., the Raman effect). In particular, future developments could demonstrate the utility of this device for detecting single particle in aqueous solutions, with very small dimensions comparable to that of viruses or proteins. Further research efforts are oriented to investigate the sensor operation as a function of different cavity lengths and different resonant orders of the PhC cavity.

References

[1] Thijs van Leest, Jeroen Heldens, Bram van der Gaag, Jaap Caro, "Photonic crystal cavities for resonant evanescent field trapping of single bacteria", Proc. SPIE 8427, Biophotonics: Photonic Solutions for Better Health Care III, 84270T (June 1, 2012).

[2] F. De Leonardis, V.M.N. Passaro “Modelling of Raman amplification in silicon-on-insulator optical microcavities”, New Journal of Physics, 9 (2007), 25, pp. 1-10.